Pilot Study to Validate Optimized Whole-Slide Images for Quality and Diagnostic Performance in Digital Pathology

Study Number:	*48-22-PATH-E*
Principal Investigator:	*Dr. John Cupp*
Co-Investigator:	*Dr. Yixiao Zhao, Val Anthony Alvero, Kenneth Tang*
Sponsor:	*Precidx Corp.*
Study Location(s):	*Hoag Memorial Hospital, Newport Beach* *Precidx Corp.*
Study Duration:	*2022/10 – 2023/04*

Abstract

The field of pathology is undergoing a digital revolution, yet challenges such as large whole-slide imaging (WSI) file sizes, costly data storage, and workflow inefficiencies persist. This study developed and validated a data optimization platform for WSI to significantly reduce file size without compromising diagnostic capabilities.

A total of hundred WSIs spanning various pathology cases were selected and digitized at Hoag Memorial Hospital (Newport Beach, CA, USA) between December 2022 and March 2023. Following acquisition, each WSI underwent processing and evaluation utilizing the Precidx Data Optimization Platform (POP). POP employed advanced algorithms to optimize image file size to identify and compress histologically relevant information from the original high-resolution image, optimizing file size for efficient storage utilization. Optimized data was standardized and reconstructed into a universally compatible TIFF format for seamless viewing and diagnosis across platforms. During evaluation, the file size reduction rate was calculated to quantitatively assess the effectiveness of the data optimization.

Objective image quality metrics such as peak signal-to-noise ratio (PSNR), structural similarity index (SSIM), and Delta-E value were also measured, as well as subjective diagnostic concordance between two pathologists.

Results from 97 valid cases showed an average file size reduction of 84.79% post-optimization. Average PSNR, SSIM, and Delta-E values were measured at 41.19 dB, 0.96, and 1.61, respectively. Both pathologists exhibited high intra-observer agreement, with a coefficient of 0.959 each, indicating consistent diagnostic interpretation with optimized WSIs.

In conclusion, this study validated the effectiveness of data optimization using POP in file size reduction while preserving diagnostic image fidelity. POP presents a promising solution for data management in digital pathology, potentially expediting the adoption of digital pathology in real-world settings.

Keywords: Pathology; Whole-slide imaging; data optimization; image quality.

Introduction

The field of pathology is undergoing a transformative shift from traditional glass slides to digital whole slide imaging (WSI) (1,2). The availability of commercial solutions for digitizing microscope slides has enabled pathologists to leverage the benefits of digital pathology. However, a significant challenge arises from the need for high magnification and detailed resolution in pathologists' diagnoses, resulting in the generation of extremely large WSI files (3,4). These prohibitively large file sizes incur exorbitant costs for WSI data storage, leading to inefficiencies in clinical workflow and expensive computation for diagnostic data analysis. In fact, the 2022 College of American Pathologists (CAP) Survey Report revealed that 84% of respondents utilizing WSI identified data storage as their largest cost, while 50% of non-users cited the deterrent of high storage fee (5). Thus, the adoption of digital pathology necessitates a comprehensive data optimization solution addressing the management of large WSI file sizes, data storage, data formats, and the integration of telepathology.

Additionally, vendor neutral archive (VNA) systems that serve as a centralized repository for medical imaging data, also require robust data management and storage solutions. Comparing to widely used picture archiving and communication systems (PACS) in radiology, such systems in digital pathology must effectively handle the vast volume and size of WSI data varies in formats and structures generated by different vendors in pathology laboratories(6). Hence, a scalable optimization solution tailored for WSI data becomes crucial for archive systems to accommodate increasing data volumes over time without compromising performance or reliability.

Beyond serving as a scalable data repository, modern cloud-based VNA systems for WSI are indispensable for telepathology services. Given the global shortage of pathologists, telepathology offers timely access to pathologic interpretations for hospital emergency rooms and healthcare facilities in rural areas lacking direct access to pathologists (7–9). Hence, a data platform capable of standardizing WSI data formats and metadata is needed to ensure compatibility and consistency in storing and

accessing WSI data. The standardization of WSIs facilitates seamless data exchange and integration across different platforms, ultimately improving diagnostic workflows and patient care outcomes.

Therefore, there is an urgent need for a comprehensive WSI data optimization platform capable of reducing large file sizes without compromising diagnostic performance while standardizing WSI data formats and metadata for the integration of digital pathology into the entire medical imaging eco system. This study aimed to develop and validate a native data optimization solution tailored for high-resolution WSI data to enable efficient and cost-effective storage and management in digital pathology. The hypothesis is that the proposed data optimization solution can significantly reduce file sizes while preserving image quality and diagnostic integrity, potentially expediting the adoption of digital pathology in real-world settings.

Material and Methods

General Methods

The study was performed at the Hoag Memorial Hospital (Newport Beach, California, USA) under specific CAP guidelines for 'validating whole slide imaging for diagnostic purposes in Pathology'. A total of 100 diverse pathology cases were collected and digitized at Hoag Hospital using the Philips IMS scanner. Each WSI was then processed using Precidx data optimization platform (POP). The effectiveness of file size reduction, objective image quality, and diagnostic integrity of the optimized WSIs were assessed. Specifically, objective image quality was evaluated using metrics such as peak signal-to-noise ratio (PSNR), structural similarity index (SSIM), and Delta-E, comparing the original and optimized digital WSIs. Diagnostic concordance was evaluated by two pathologists, Dr. John Cupp and Dr. Lee Thomas, each with over 15 years of experience in pathology. This subjective evaluation aimed to determine the level of agreement between diagnoses made using the original and optimized WSIs, providing insights into the diagnostic integrity of the optimized images.

Data Inclusion and Exclusion Criteria

A total of 100 cases were enrolled in the validation study, with three cases being excluded due to mislabeling on the original glass slides. The sampled biopsies represented diverse malignancies, including breast cancer, colorectal cancer, lung cancer, brain tumors, thyroid disorders, etc., as detailed in **Table 1**. Of the 97 cases included, 66 were positive for various cancer types, including adenocarcinoma, metastatic adenocarcinoma, squamous cell carcinoma, carcinoma, fibroadenoma, glioblastoma, and melanoma, among others, as outlined in **Table 2**.

Table 1. Case Demographics and Biopsy Types

Tissue Sample	Count
Breast	6
Colorectal	12
Prostate	2
Bladder	7
Brain	5
GI	6
Thyroid	5
Pancreas	4
Lung	14
Bronchiectasis	2
Arm	6
Omen tum	11
Tonsillar	4
Axillary lymphadenopathy	12
Cervical lymphadenopathy	1
Total	**97**

Table 2. Cancer Types for Positive Cases

Cancer Type	#Count
fibroadenoma	1
carcinoma	22
adenocarcinoma	14
metastatic adenocarcinoma	5
glioblastoma	2
melanoma	5
squamous cell carcinoma	3
metastatic colon cancer	3
fibromatosis	1
others	10
Total	**66**

Additionally, a variety of immunohistochemistry (IHC) stains and markers were applied, including 33 cases of hematoxylin and eosin (H&E) stain, serial sections with target stains such as differentiation

markers (p40, p53, p63, etc.), epithelial markers (CDX, CK5/6, CK7, CK20, etc.), prognostic markers (Ki67, MLH1, MSH2, MSH6, etc.), all of which are specified in **Table 3**.

Table 3. Immunohistochemistry (IHC) Stains and Markers

Markers	Stains	#Count
Hematoxylin and eosin (H&E) stain	HE	31
Breast Markers	PAX8	2
	ER	1
	GATA3	2
	Her2	1
Differentiation Markers	p40	1
	p53	1
	p63	2
	PAP	2
Epithelial Markers	CDX2	2
	CK5.6	2
	CK7	4
	CK20	6
	EMA	1
	SOX10	2
	TTF1	3
	Pankeratin	3
	Napsin	2
Hematopoietic Markers	CD3	1
	CD5	1
	CD20	1
Melanocytic Markers	MelanA	1
	S100	2
Nervous System Markers	GFAP	1
Neuroendocrine Markers	Synaptophysin	3
Prognostic Markers	p16	2
	WT1	2
	MLH1	1
	MSH2	1
	MSH6	1
	Ki67	2
Others	BCL1	1
	CGMS	1
	GMS	1

	HE(Smear)	1
	HMB45	1
	IDH1	1
	PMS2	1
	PR	1
	SOX11	1
	Villin	1
Total		**97**

Precidx Data Optimization Platform (POP)

After data acquisition, each proprietary digital WSI was standardized and optimized using Precidx Data Optimization Platform (**Figure 1**). Specifically, the WSI image data and the associated metadata were stored and managed separately in the image and metadata databases. The associated metadata such as image dimension, tile dimension, resolution, level, color profiles and correction, were automatically extracted from the proprietary WSI data and saved into a standardized metadata for querying and management. The patient-associated metadata was anonymized and tokenized at the mean time during the process. Additionally, thumbnail image was generated for image preview.

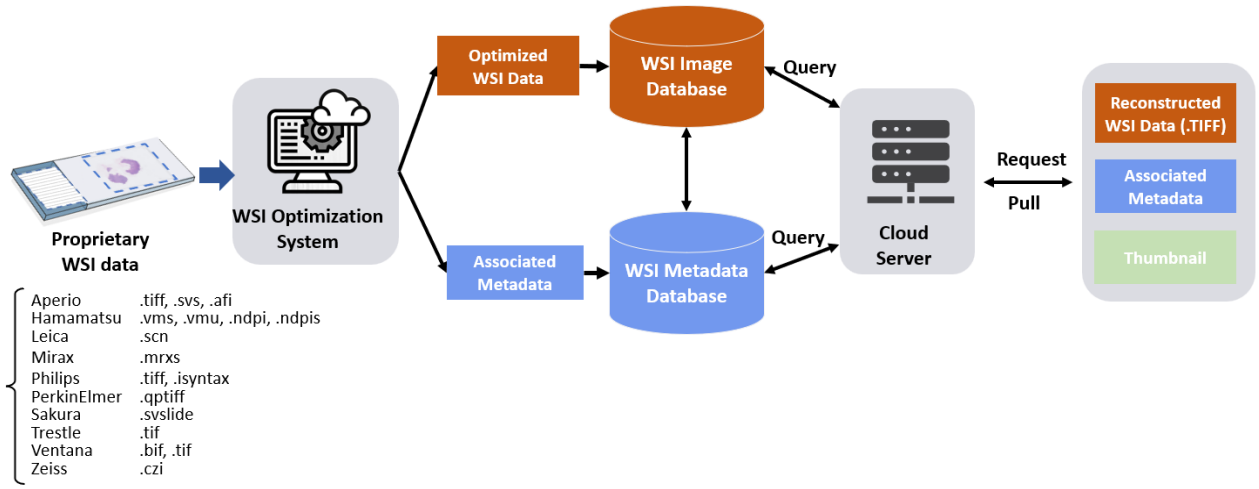

Figure 1. A framework of WSI data optimization platform and cloud server.

For the image optimization process, a single layer of high-resolution WSI was first extracted from the original pyramidal WSI, as described in **Figure 2**. Next, the histological relevance of each single tile

was calculated based on local binary patterns (LBPs) of its lower band image from the discrete wavelet transform. All tiles that contain histological information were compressed at a high image quality while the noninformative relevant tiles were compressed at a lower image quality using a lossy compression algorithm. The proposed POP compression approach utilized the predictive coding and entropy optimizations to reduce redundancy more intelligently than JPEG's brute-force DCT, yielding smaller files with fewer visible artifacts, especially improved for sharp edges and gradients in the field of digital pathology. Such approach predicts pixel values block using one of several directional modes (e.g., copying pixels from the top, left, or a gradient), which exploits spatial redundancy before DCT-like transformation used in JPEG compression. Only the difference (residual) between the predicted and actual pixels undergoes frequency-domain compression (similar to DCT but with better context). Also, unlike JPEG's rigid 8×8), **variable block sizes** (e.g. 4×4 to 16×16 blocks) were used to reduce artifacts in complex areas. While superior to JPEG's effectiveness and avoiding JPEG2000's complexity, the POP approach requires more computational effort during encoding. As a result, a sequence of POP encoded image tiles were stored in the WSI image database for storage use (**Figure 2**).

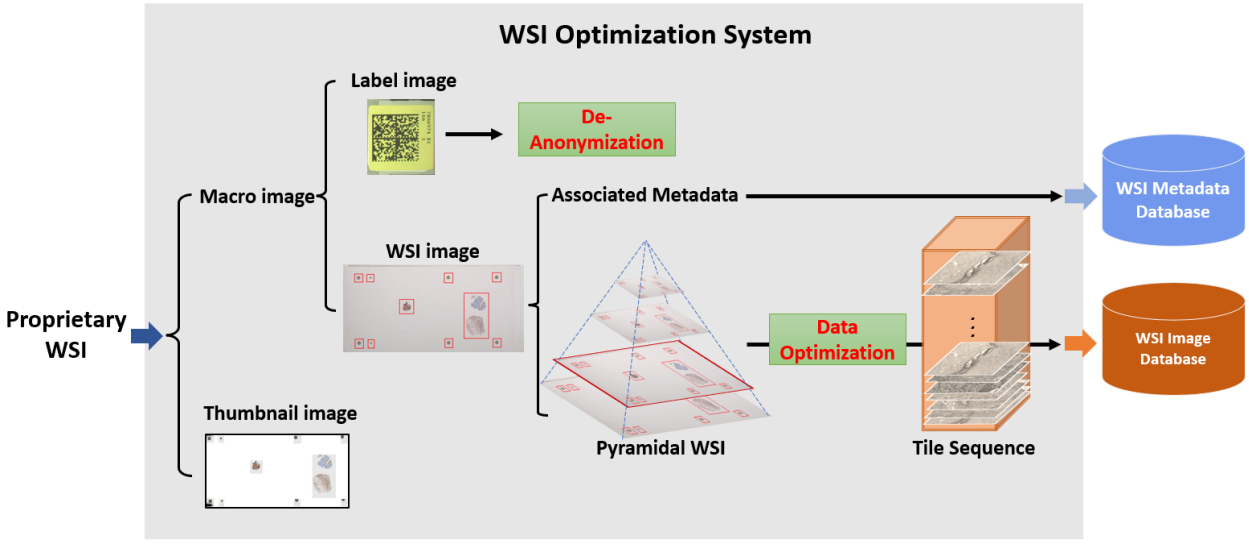

Figure 2. WSI data optimization platform with de-anonymization and image data optimization processes.

For data retrieval, each tile from the sequence was first decoded and patched to a single—layer image as the base of the reconstructed pyramidal WSI. Multiple intermediate layers were generated for the reconstruction of the pyramidal WSI, using native WSI image parameters recorded in the metadata. Such decompressed WSI can be written into a generic TIFF format, DICOM WSI format, or other proprietary WSI formats depending on the use case. All formats support zooming and panning functionalities for seamless navigation during visualization and clinical diagnostic interpretation. The hierarchical structure allows for efficient access to varying levels of magnification, enabling detailed examination of tissue structures and pathological features.

Assessment of Storage Saving and Image Quality

To evaluate the performance of optimized WSIs, several evaluation metrics were used to measure both storage efficiency and image quality. These metrics include:

File size reduction ratio (FSRR): This metric quantifies the reduction in file size achieved through optimization, expressed as a percentage of the original file size:

$$FSRR = \frac{(\text{original file size} - \text{optimized file size})}{\text{original file size}} \times 100\%$$

Peak signal-to-noise ratio (PSNR): PSNR measures the quality of the optimized image by comparing it to the original image. It quantifies the ratio between the maximum possible power of a signal (the original image) and the power of the noise (the difference between the original and compressed images). Higher PSNR values indicate better image quality. PSNR is typically used to correlate with human perception of image quality, particularly for lossy compression methods. For 8-bits images, PSNR values typically range from 25 to 50 dB (10,11) in lossy image compression, with a PSNR above 40 dB indicating near-imperceptible differences for human eyes(12,13).

Structural Similarity Index (SSIM): SSIM assesses the similarity between the original and optimized images in terms of luminance, contrast, and structure (14–17). It compares local patterns of pixel intensities and aims to measure perceived changes in structural information. SSIM produces a value between -1 and 1, where 1 indicates perfect similarity. Unlike PSNR, SSIM takes into account human visual perception and is often considered more accurate in predicting perceived image quality, especially for images subjected to lossy compression.

DeltaE: DeltaE measures the color difference between the original and optimized images as perceived by the human eye (18). DeltaE values are typically used in applications where color fidelity is critical (19). Defined by the International Commission on Illumination (CIE), DeltaE is used to standardize color in colorimetry, photometry, and imaging. Lower DeltaE values indicate minimal perceptible difference, while higher values suggest noticeable color variation. The values range from 0 to 100 with DeltaE values below 1 being imperceptible, 1-2 perceptible with close observation, and 2-10 perceptible at a glance (20–22).

Assessment of Diagnostic Concordance

The assessment of diagnostic concordance between native and optimized WSIs involved a systematic approach to ensure unbiased and accurate assessments.

Pathologist Review Protocol: Two pathologists independently and blindly reviewed both original and optimized WSIs without prior knowledge of the images' origin or characteristics. Each pathologist underwent two rounds of review to assess intra-observer reliability. A washout period of three weeks was implemented between the first and second viewings of the same WSI as required by WSI validating guidelines (23,24). The washout period prevented potential recall bias and allowed pathologists to approach each case with a fresh perspective during subsequent reviews. In cases

where pathologists had divergent opinions after the initial two rounds of review, they collaborated for a third round of review to reach a consensus diagnosis at the end of the study.

Randomized Case Distribution: A total of 200 cases, comprising 100 native WSIs and 100 optimized WSIs, underwent a randomized assignment into two groups—Group A and Group B. The randomization process guaranteed an equitable distribution of cases from both native and optimized WSIs, eliminating any bias in case selection. Each pathologist independently reviewed a 100-case test set in a random order, with only one group of the dataset accessible during assessment to prevent biases influenced by exposure to subsequent cases.

WSI Rating System: A nuanced four-point rating system was employed to assess diagnostic concordance and confidence. The scale ranged from non-diagnostic quality (0) to definitely positive (3). Noted that the assigned score reflected the confidence of diagnosis rather than the inherent quality of the image, emphasizing the importance of evaluating diagnostic findings over technical image characteristics. The rating scale is delineated as follows:

- 0 - Non-diagnostic quality: Image quality insufficient for reliable diagnosis; lacks information for condition determination.
- 1 - Definitely negative: No evidence of the diagnosed condition; absence of abnormality or disease.
- 2 - Hard to define: negative to positive: Characteristics challenging to classify definitively; may require further evaluation for conclusive diagnosis.
- 3 - Definitely positive: Clear demonstration of the diagnosed condition; definitive indicators of abnormality or disease.

Evaluation of Diagnostic Concordance: Both intra-observer reliability and intra-observer variability were assessed using Cohen's kappa coefficient. For the intra-observer reliability, Cohen's kappa was used to assess the consistency of ratings or diagnoses made by the same pathologists, quantifying the level of

agreement between the pathologist's ratings during repeated reviews (25). For the inter-observer variability, the ratings provided by each pathologist were compared pairwise to determine the level of agreement. The observed agreement (the proportion of ratings that agree between observers) is compared to the expected agreement (the proportion of agreement that would be expected by chance alone). Cohen's kappa ranges from -1 to 1, where higher values signify stronger agreement between observers, while values close to 0 indicate agreement equal to chance or worse. Kappa values greater than 0.6 generally indicate substantial agreement beyond chance; greater than 0.8 indicates almost perfect agreement in diagnostic interpretations.

Evaluation of Diagnostic Performance: The consensus diagnosis of the two pathologists was considered to be the reference standard of each case. True positive (TP), true negative (TN), false positive (FP), and false negative (FN) cases are calculated for each data group (native and optimized WSIs) of each pathologist. The metrics of accuracy, specificity, sensitivity, positive predictive value (PPV), negative predictive value (NPV) were then calculated based on these TP, TN, FP, and FN values for each pathologist and each data group.

Statistical Analysis

The average file size reduction rate between the original and optimized WSIs were computed to quantify the effectiveness of the optimization. Objective image quality was then evaluated by comparing the average and standard deviation of the PSNR, SSIM, and Delta-E values between the native and optimized WSI. To evaluate the diagnostic concordance, the Cohen's kappa coefficient was employed, quantifying both intra-observer reliability (κ_{intra}) and inter-observer variability (κ_{inter}). The Mann-Whitney U test was also used for the statistical assessment of the disparities observed in the evaluations conducted by different pathologists. Additionally, the diagnostic performance of each pathologist was evaluated using metrics such as accuracy, sensitivity, and specificity.

Results

Qualitative Analysis

An example of a whole slide image optimized and reconstructed using the data optimization platform is presented in **Figure 3**. The image was dyed by the H&E stain and five different resolutions (magnifications) are showed in 16 µm/pixel (~x/2), 4 µm/pixel (~2x), 1 µm/pixel (~10x), 0.5 µm/pixel (~20x), and 0.25 µm/pixel (~40x) .

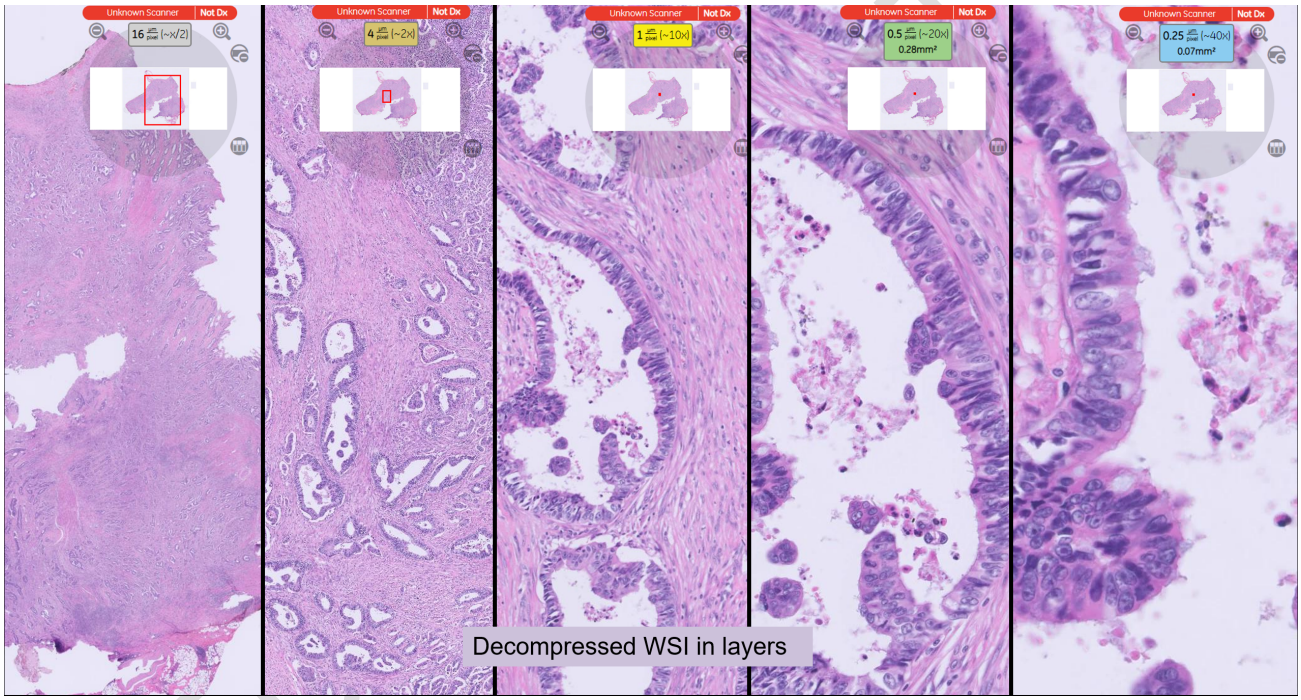

Figure 3. An example of the optimized WSI using H&E stain, with the various resolutions (magnifications):16 µm/pixel (~x/2), 4 µm/pixel (~2x), 1 µm/pixel (~10x), 0.5 µm/pixel (~20x), and 0.25 µm/pixel (~40x) (left to right).

Representative examples of the original and optimized WSIs from three different tissue samples and stains are displayed in **Figures 4-6**.

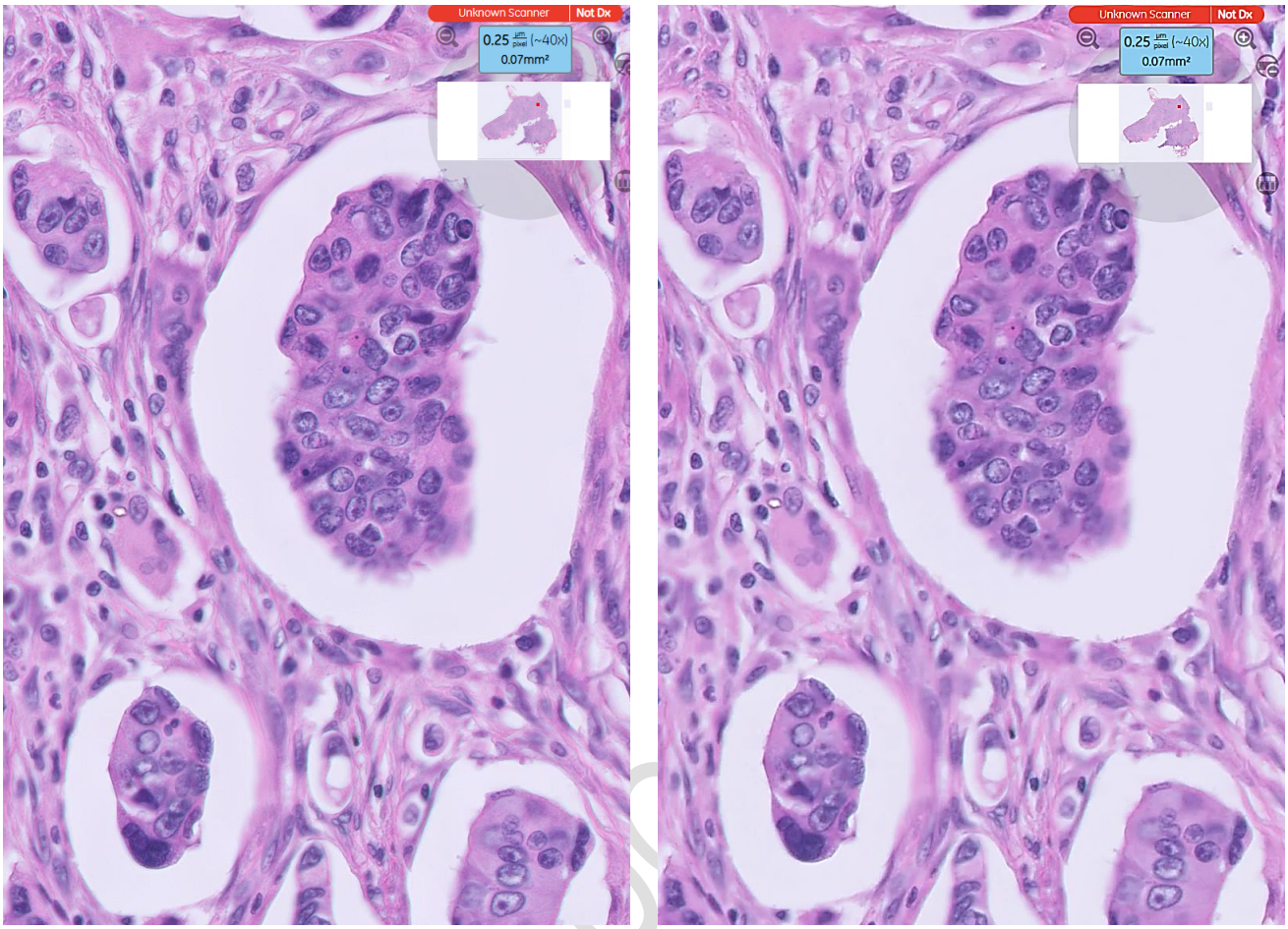

a) b)

Figure 4. A 4.2 cm obstructing sigmoid colon mass of a 74-year-old male stained by H&E stain. a) Original WSI, b) Optimized WSI are both at the magnification of 40x with the resolution of 0.25 µm/pixel. The original file size and the optimized file size are 1.68 Gb and 287.39 Mb, respectively, with the FSRR at 82.91%. The PSNR, SSIM and DeltaE are 39.77, 0.95 and 1.89, respectively.

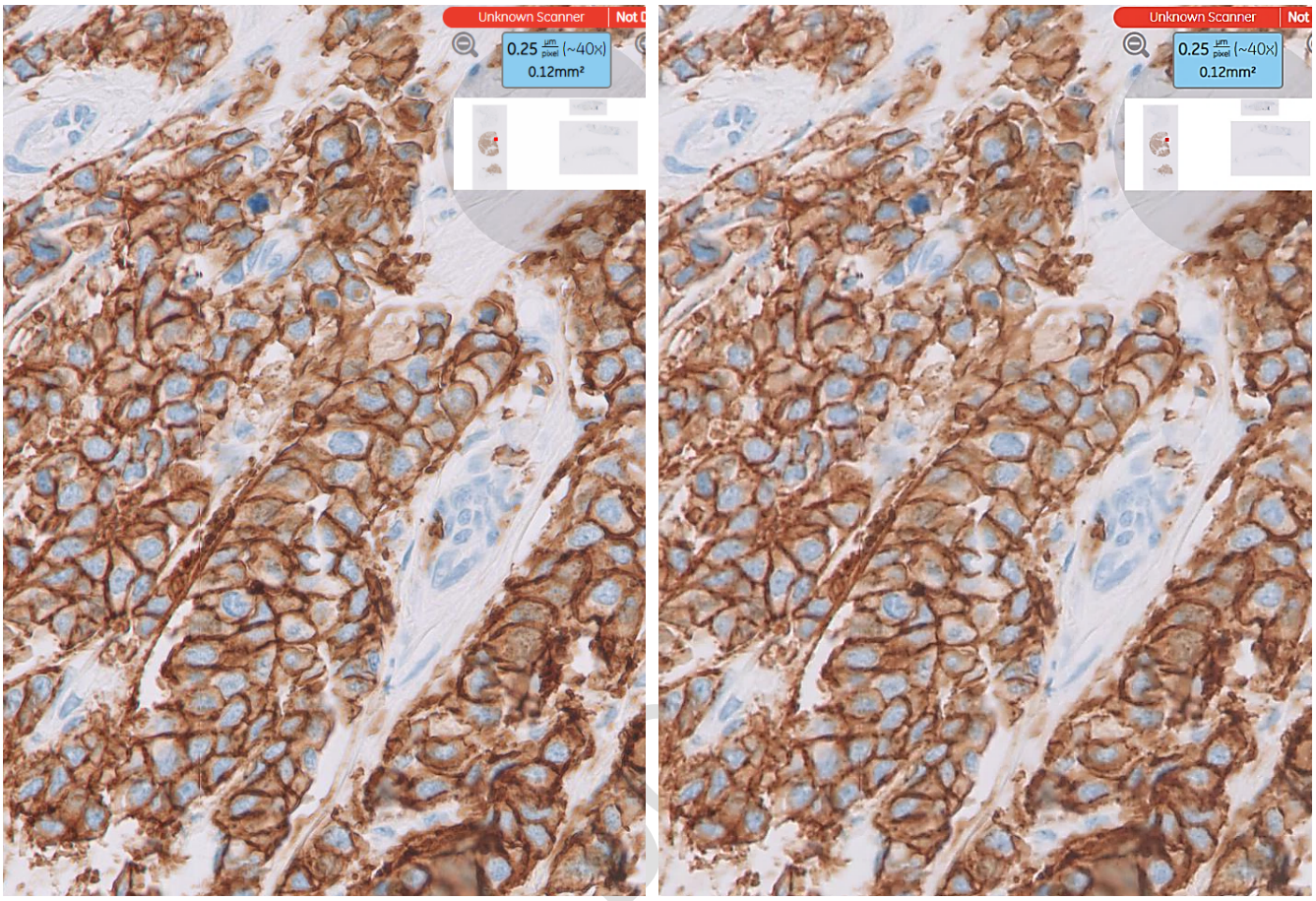

a) b)

Figure 5. An irregular right breast mass of a 43-year-old female stained by the HER2 stain. a) Original WSI, b) Optimized WSI are both at the magnification of 40x with the resolution of 0.25 µm/pixel. The original file size and the optimized file size are 637.35 MB and 98.03 Mb, respectively, with the FSRR at 84.62%. The PSNR, SSIM and DeltaE are 39.39, 0.95 and 1.96, respectively.

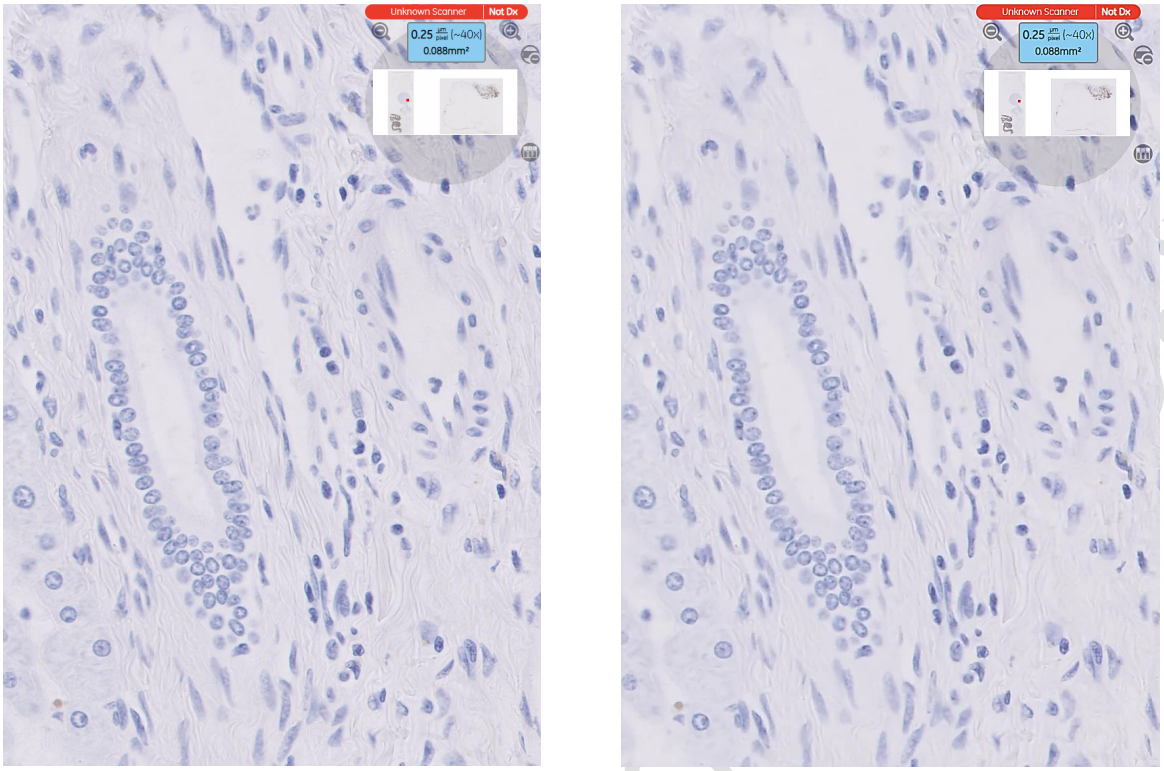

a) b)

Figure 6. A right upper arm skin lesion of an 82-year-old female stained by CK20 stain. a) Original WSI, b) Optimized WSI are both at the magnification of 40x with the resolution of 0.25 µm/pixel. The original file size and the optimized file size are 1.39 Gb and 183.50 Mb, respectively, with the FSRR at 87.15%. The PSNR, SSIM and DeltaE are 43.26, 0.97 and 1.22, respectively.

Quantitative Analysis

Objective Image Quality Metrics

Overall, the file sizes of the 97 valid original WSIs ranged from 138.42 MB to 3.41 GB, with 48 cases less than 1 GB and 49 cases larger than 1 GB. After optimization, the file sizes for storage ranged from 9.18 MB to 795.05 MB.

On average, the file size reduction achieved was 84.79% with a standard deviation of 3.95%. The minimum file size reduction rate was found to be 76.10%, while the maximum reduction reached 94.08%. The distribution of file size reduction rates is illustrated in **Figure 7**.

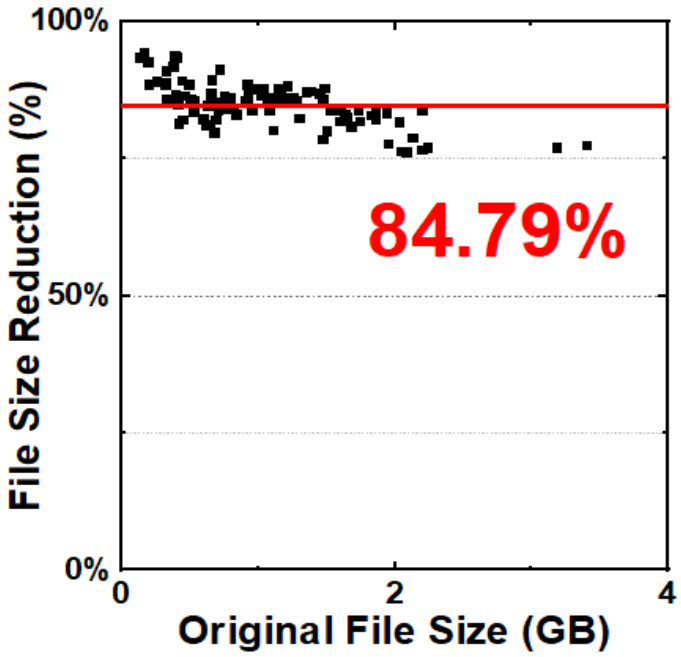

Figure 7. File size reduction rate per file.

Regarding objective image metrics, the PSNR averaged at 41.19 dB with a standard deviation of 2.01 dB. The SSIM yielded an average of 0.96 with a standard deviation of 0.01. Additionally, the average Delta-E value was found to be 1.61 with a standard deviation of 0.38. Further details of the objective image metrics within specific file size ranges are presented in Table 4.

Table 4: Objective image metrics evaluation

File size range	< 1 GB	>1 GB	ALL
Number of cases	48	49	97
File Size Reduction Rate	86.44%	83.16%	84.78%
PSNR	41.66	40.72	41.19
SSIM	0.97	0.96	0.96
DeltaE	1.56	1.67	1.61

Subjective Diagnostic Concordance

The inter-observer variability between two pathologists and Intra-observer reliability for each pathologist are detailed in **Table 5** and **6**, respectively.

For the two pathologists, the diagnostic agreement of original and optimized cases was found to be 0.887 and 0.928, respectively. Additionally, the intra-diagnostic agreement of both pathologist A and B was measured at 0.959, demonstrating high consistency in their individual assessments. The kappa values of the inter-observer variability and intra-observer reliability were all above 0.7, indicating substantial to almost perfect agreement among observers.

Table 5: Inter-observer variability: Original vs. Optimized WSI

	Original	**Optimized**
Agreement	0.887	0.928
Kappa value	0.753	0.841
p-value	0.765	0.163

- *Note: Kappa value greater than 0.70 indicates the inter-observer variability is satisfactory*
- *p-value less than 0.05 indicates significant difference.*

Table 6: Intra-observer reliability: Pathologist A vs. Pathologist B

	Pathologist A	**Pathologist B**
Agreement	0.959	0.959
Kappa value	0.908	0.911
p-value	0.045	0.783

- *Note: Kappa value greater than 0.70 indicates the intra-observer reliability is satisfactory*
- *p-value less than 0.05 indicates significant difference.*

Among 66 positive cases and 31 negative cases, the results demonstrate that both pathologists achieved high accuracy, sensitivity, and specificity rates above 90% for both native and optimized datasets, as shown in **Table 7**. Overall, the results suggest robust diagnostic performance across different datasets and indicate the effectiveness of the optimization process in maintaining diagnostic accuracy.

Table 7： Diagnostic Performance Metrics: Pathologist A vs. Pathologist B

	Pathologist A		Pathologist B	
	Original	**Optimized**	**Original**	**Optimized**
Sensitivity	0.939	1.000	0.924	0.984
Specificity	1.000	1.000	0.936	0.967
NPV	0.886	1.000	0.853	0.967
PPV	1.000	1.000	0.968	0.984
Accuracy	0.956	1.000	0.928	0.978

- *Note: NPV: negative predictive value; PPV: positive predictive value*

Conclusion

In conclusion, this study tackled the challenges associated with large whole-slide imaging (WSI) file sizes, high data storage costs, and workflow inefficiencies in the field of pathology through the development and validation of a WSI data optimization system (POP). The proposed solution significantly reduced file size while preserving diagnostic performance, leveraging advancements in image optimization.

The POP system implemented a series of processes, including the management of metadata, the extraction of high-resolution WSI image, identification of histologically relevant information, and application of image compression techniques, all contributing to a substantial reduction in file size without compromising diagnostic image quality. Furthermore, the standardized format of the reconstructed WSIs in a generic TIFF ensures seamless integration into existing diagnostic workflows across different platforms.

Evaluation of the optimized WSIs revealed an impressive 84.79% reduction in file size, with average PSNR, SSIM, and Delta-E values indicating high-quality images suitable for diagnostic interpretation. Additionally, the inter- and intra- diagnostic concordance was preserved after the image optimization. The optimized WSIs showed high sensitivity and specificity, further validating the effectiveness of the optimization system in preserving diagnostic accuracy.

Overall, this research validated the effectiveness of the proposed WSI data optimization system in overcoming challenges associated with large file sizes while maintaining diagnostic performance and standardizing WSI data formats. The implementation of POP offers a more accessible, scalable, and cost-effective solution for data storage in digital pathology, potentially revolutionizing the practice of pathology and improving healthcare delivery on multiple fronts.

Reference

1. Romero Lauro G, Cable W, Lesniak A, Tseytlin E, McHugh J, Parwani A, et al. Digital Pathology Consultations—a New Era in Digital Imaging, Challenges and Practical Applications. J Digit Imaging. 2013 Aug;26(4):668–77.

2. Abels E, Pantanowitz L. Current State of the Regulatory Trajectory for Whole Slide Imaging Devices in the USA. J Pathol Inform. 2017;8:23.

3. Indu M, Rathy R, Binu M. "Slide less pathology": Fairy tale or reality? J Oral Maxillofac Pathol. 2016;20(2):284–8.

4. Corredor G, Romero E, Iregui M. An adaptable navigation strategy for Virtual Microscopy from mobile platforms. Journal of Biomedical Informatics. 2015 Apr 1;54:39–49.

5. Vernon L, Analylics S, DeLisle A, Cohen MB, Eakin SM, Battistone A, et al. 2022 Practice Characteristics Survey Report. :53.

6. Farahani N, Parwani AV, Pantanowitz L. Whole slide imaging in pathology: advantages, limitations, and emerging perspectives. PLMI. 2015 Jun 11;7:23–33.

7. Ghosh A, Brown GT, Fontelo P. Telepathology at the Armed Forces Institute of Pathology: A Retrospective Review of Consultations From 1996 to 1997. Archives of Pathology & Laboratory Medicine. 2018 Feb 1;142(2):248–52.

8. Horbinski C, Fine JL, Medina-Flores R, Yagi Y, Wiley CA. Telepathology for intraoperative neuropathologic consultations at an academic medical center: a 5-year report. J Neuropathol Exp Neurol. 2007 Aug;66(8):750–9.

9. Vitkovski T, Bhuiya T, Esposito M. Utility of telepathology as a consultation tool between an off-site surgical pathology suite and affiliated hospitals in the frozen section diagnosis of lung neoplasms. Journal of Pathology Informatics. 2015 Jan 1;6(1):55.

10. Faragallah OS, El-Hoseny H, El-Shafai W, El-Rahman WA, El-Sayed HS, El-Rabaie ESM, et al. A Comprehensive Survey Analysis for Present Solutions of Medical Image Fusion and Future Directions. IEEE Access. 2021;9:11358–71.

11. Chervyakov N, Lyakhov P, Nagornov N. Analysis of the Quantization Noise in Discrete Wavelet Transform Filters for 3D Medical Imaging. Applied Sciences. 2020 Jan;10(4):1223.

12. Kim J, Lee J, Lee S, Lee M. Development of 3-D stereo endoscopic PACS viewer. In: ISIE 2001 2001 IEEE International Symposium on Industrial Electronics Proceedings (Cat No01TH8570). 2001. p. 278–80 vol.1.

13. Lalithakumari S, Pandian R, Rani J, Vinothkumar D, Sneha A. Selection of optimum compression algorithms based on the characterization on feasibility for medical image. Biomed Res. 2017;28(13):5.

14. Wang Z, Bovik AC, Sheikh HR, Simoncelli EP. Image Quality Assessment: From Error Visibility to Structural Similarity. IEEE Trans on Image Process. 2004 Apr;13(4):600–12.

15. Setiadi DRIM. PSNR vs SSIM: imperceptibility quality assessment for image steganography. Multimed Tools Appl. 2021 Mar 1;80(6):8423–44.

16. Channappayya SS, Bovik AC, Caramanis C, Heath RW. SSIM-optimal linear image restoration. In: 2008 IEEE International Conference on Acoustics, Speech and Signal Processing. 2008. p. 765–8.

17. Zhang L, Zhang L, Mou X, Zhang D. A comprehensive evaluation of full reference image quality assessment algorithms. In: 2012 19th IEEE International Conference on Image Processing. 2012. p. 1477–80.

18. Backhaus W, Kliegl R, Werner JS. Color Vision: Perspectives from Different Disciplines. Walter de Gruyter; 1998. 366 p.

19. Delta E 101 [Internet]. [cited 2022 Nov 15]. Available from: http://zschuessler.github.io/DeltaE/learn/

20. Brainard DH. 5 - Color Appearance and Color Difference Specification. In: Shevell SK, editor. The Science of Color (Second Edition) [Internet]. Amsterdam: Elsevier Science Ltd; 2003 [cited 2022 Nov 15]. p. 191–216. Available from: https://www.sciencedirect.com/science/article/pii/B9780444512512500064

21. Shrestha P, Hulsken B. Color accuracy and reproducibility in whole slide imaging scanners. JMI. 2014 Jul;1(2):027501.

22. Useful Color Equations [Internet]. [cited 2022 Nov 15]. Available from: http://www.brucelindbloom.com/

23. Pantanowitz L, Sinard JH, Henricks WH, Fatheree LA, Carter AB, Contis L, et al. Validating whole slide imaging for diagnostic purposes in pathology: guideline from the College of American Pathologists Pathology and Laboratory Quality Center. Arch Pathol Lab Med. 2013 Dec;137(12):1710–22.

24. Evans AJ, Brown RW, Bui MM, Chlipala EA, Lacchetti C, Milner DA, et al. Validating Whole Slide Imaging Systems for Diagnostic Purposes in Pathology. Archives of Pathology & Laboratory Medicine. 2022 Apr 1;146(4):440–50.

25. McHugh ML. Interrater reliability: the kappa statistic. Biochem Med (Zagreb). 2012;22(3):276–82.